

## Article

# Hybrid Printing of Silver-Based Inks for Application in Flexible Printed Sensors

Jakub Krzemiński <sup>1,\*</sup>, Dominik Baraniecki <sup>1</sup>, Jan Dominiczak <sup>1</sup> , Izabela Wojciechowska <sup>1</sup>, Tomasz Raczyński <sup>1</sup>, Daniel Janczak <sup>2</sup> and Małgorzata Jakubowska <sup>2</sup>

<sup>1</sup> Centre for Advanced Materials and Technologies CEZAMAT, Warsaw University of Technology, 00-661 Warsaw, Poland

<sup>2</sup> Faculty of Mechatronics, Institute of Metrology and Biomedical Engineering (IMIB), Warsaw University of Technology, 00-661 Warsaw, Poland

\* Correspondence: jakub.krzeminski@pw.edu.pl

**Abstract:** This study explores the potential benefits of combining different printing techniques to improve the production of flexible printed sensors, which is a relevant application for modern coating and surface design. The demand for cheap, flexible, precise, and scalable sensors for wearable electronics is increasing, and printed electronics techniques have shown great potential in meeting these requirements. To achieve higher performance and synergy, the paper introduces the concept of hybrid printing of electronics by combining aerosol jet printing and screen printing. This multi-process approach allows for large-scale production with high printing precision. The study prepares hybrid connections on a flexible substrate foil for use in flexible printed sensor manufacturing. The research team tests different combinations of printed layers and annealing processes and finds that all prepared samples exhibit high durability during mechanical fatigue tests. Surface morphology, SEM images, and cross-section profiles demonstrate the high quality of printed layers. The lowest resistance among the tested hybrid connections obtained was 1.47 Ω. The study's findings show that the hybrid printing approach offers a novel and promising solution for the future production of flexible sensors. Overall, this research represents an interdisciplinary approach to modern coating and surface design that addresses the need for improved production of wearable electronics. By combining different printing techniques, the study demonstrates the potential for achieving high-volume production, miniaturization, and high precision, which are essential for the ever-growing market of wearable sensors.

**Keywords:** screen printing; aerosol jet printing; printed electronics; coatings; functional materials



**Citation:** Krzemiński, J.; Baraniecki, D.; Dominiczak, J.; Wojciechowska, I.; Raczyński, T.; Janczak, D.; Jakubowska, M. Hybrid Printing of Silver-Based Inks for Application in Flexible Printed Sensors. *Crystals* **2023**, *13*, 720. <https://doi.org/10.3390/cryst13050720>

Academic Editor: George D. Verros

Received: 31 March 2023

Revised: 18 April 2023

Accepted: 21 April 2023

Published: 24 April 2023



**Copyright:** © 2023 by the authors. Licensee MDPI, Basel, Switzerland. This article is an open access article distributed under the terms and conditions of the Creative Commons Attribution (CC BY) license (<https://creativecommons.org/licenses/by/4.0/>).

## 1. Introduction

Flexible and stretchable printed electronics are becoming increasingly present in human life with solutions for healthcare [1,2], photovoltaics [3,4], wearable solutions [5–8], sensors [9–12], and many other electronics-related applications [13,14]. There is a substantial amount of printing techniques employed in the fabrication of flexible printed electronics.

Screen printing is one of the most widely used contact printing techniques that allow for highly scalable production. This printing method can be used to produce pressure sensors [9] as well as chemical sensors [10]. However, conventional screen printing is not suitable for 3D applications [15] and there are resolution limitations. A resolution of 100 μm is achievable and considered to be a good resolution. However, it can be lowered to less while requiring optimization processes and screens with steel mesh [4,16].

Among the contactless printing techniques, devoid of some of the limitations of screen printing, is aerosol jet printing (AJP). This printing technique is widely represented in recent flexible electronics solutions [2,7,17,18]. Aerosol jet printing enables a printing resolution of 10 μm [19], which is superior to screen printing. Moreover, the technique is used in

printing on 3D substrates with protrusions and inclusions, as well as on the surface of the device casing [20–22].

The above-mentioned techniques were used separately in countless solutions. The hybrid connection may be used in applications by certain research facilities. However, there is hardly any research regarding a combination of printing methods. This may result from the lack of access of individual research facilities to the equipment of both printing techniques or from the low demand to combine these techniques in current applications. This work is meant to prove that the connection of screen printing with aerosol jet printing is viable for application in flexible electronics, as well as to investigate the properties of the hybrid connection of the techniques.

Among the anticipated use cases for hybrid printing is the possibility of printing aerosol patterns of high resolution to increase the resolution of the screen print. While techniques such as InkJet and laser ablation allow for a high precision layer production, AJP allows for printing on various substrates, including 3D substrates. It is also a non-contact printing method. AJP will allow micrometer-sized tracks to be deposited, providing an electrical connection between screen-printed contacts while increasing repeatability and scalability through the advantages that screen printing offers.

Additionally, significant is the opportunity for aerosol jet printing on 3D substrates. Layers deposited on flat surfaces by screen printing can then be connected via AJP. Additionally, the use of AJP to make vias in electronics is known [23]. In a hybrid combination, this can enable the joining of double-sided screen-printed layers through AJP deposition inside the micro-holes.

As no research regarding the combined printing of the techniques exists, this work examined the electrical properties and the surface morphology of the hybrid connections. To check the flexibility of the printed layers, a mechanical fatigue test was conducted.

It was also essential to examine the influence of the printing sequence of the respective printing techniques. The sequence of printing a screen-printed layer on top of the AJP print could result in damaging the AJP print due to squeegee movement pressure on the AJP lines. Additionally, the desire arose to investigate the properties of AJP printing on a surface with a screen-printed layer, but with a single drying process after both prints have been deposited. It is regarded as a means of speeding up the printing process on the production line. Here, a concern emerged about superficial drying of the screen-printed layer which could lead to a faulty hybrid bond, resulting from an overly long time between printings.

## 2. Materials and Methods

### 2.1. Materials

The printed hybrid connections were fabricated based on a predefined design (Figure 1), which was tailored to accommodate the 4-wire sensing method for resistance measurement of the connection and the aerosol jet printed (AJP) line. The design was optimized considering the width of the screen-printed layers (1 mm) and the width of the AJP lines (approximately 50–70  $\mu\text{m}$ ). As a result, the overlap area in the hybrid connection took on a rectangular shape with dimensions corresponding to the widths. This configuration ensured accurate and precise resistance measurements, taking into account the specific dimensions of the printed layers and lines involved in the hybrid connection.

Two screen printing pastes were selected for the research. A commercial screen printing paste LOCTITE<sup>®</sup> ECI 1010 was selected due to its high conductivity and use in flexible electronics solutions [12,24]. Additionally, a dedicated silver paste was developed for the research. The composition contained 70 wt% of silver flakes from Amepox<sup>™</sup> (~2–8  $\mu\text{m}$  width) in a polymethylmethacrylate-based (PMMA-based) carrier described in other works [25]. In the following, the pastes will be referred to as ECI 1010 and PMMA, respectively. A Brookfield<sup>™</sup> Rheometer was used to measure the rheology of the pastes (Figure 2). Differences between the materials can be observed with PMMA-based paste presenting greater viscosity ~8 Pa·s than ECI 1010 ~4 Pa·s at 150 1/s shear rate which is relevant to the used screen printing flood speed of 150 mm/s. In addition, PMMA-based

paste has a significantly greater thixotropy with the slump area at 40 Pa·s which is 10x higher than ECI 1010.

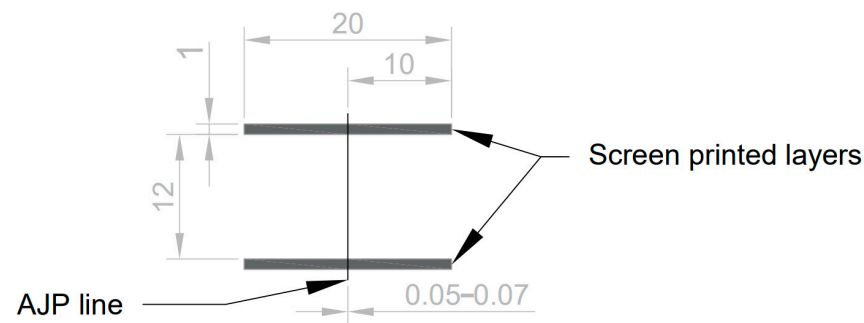


**Figure 1.** Design of the printed layers: gray stripes represent the screen-printed layer (width of 1 mm); the black line represents the AJP printed line (width of 50–70  $\mu\text{m}$ ). All dimensions displayed are in millimeters [mm].

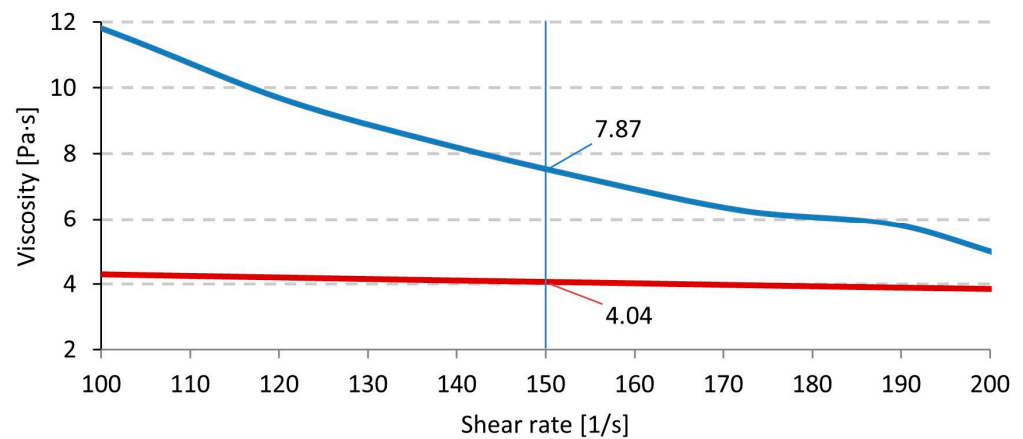


**Figure 2.** Rheology of the pastes for screen printing as a plot of viscosity (Pa·s) over shear rate (1/s). Displayed are: LOCTITE® ECI 1010 (blue curve); PMMA-based silver paste (red curve).

For the AJP printed lines, one commercial material was selected—a Ag-based ink from UT Dots: Ag40X (UTD40X). This ink was used as its properties have been previously investigated [3], and it has proved to be a reliable material for application in flexible solutions [26–28].

The materials were selected from a wide range of materials for conductive silver-based prints. From among them the three most used, comparable, and compatible were selected.

The use of metallic aerosol inks requires an annealing temperature of 250 °C to achieve better conductivity [3], therefore, the use of a high-temperature-resistant film was necessary to conduct the research. Kapton polyimide film was chosen as the substrate material for the prints due to its high temperature resistance. This is also a material commonly used in flexible printed electronics applications [29–31]. Other materials could be used to broaden the research, but the process would require some optimization considering the necessity of the high temperature annealing of the metallic based coatings.

## 2.2. Fabrication and Measurements

In the research, an AUREL C920 screen printer was used for printing the layers. For the printing process, squeegee pressure was set at around 64 N and the forward printing speed was 150 mm/s. Polyester screens masked with photo emulsion for screen printing with mesh 77T were used for the fabrication of screen printed layers.

An Optomec® Aerosol jet Printer was used for the deposition process of the AJP lines. Atomization of the ink was conducted with the ultrasonic atomizer. The following

printing parameters were used: sheath flow 20 SCCM, atomization flow 20 SCCM, heat table temperature 60 °C, and printing velocity 2 mm/s. AJP prints of 2 and 4 layers were tested in this study.

The prints were annealed in a Czylok muffle chamber furnace at 250 °C for 1 h. The samples have been inserted into a preheated chamber and the time of firing was measured from the moment the set temperature of 250 °C was achieved. The annealing of the samples was a necessary process to improve the performance of the silver conductive layers, enhance conductivity, and ensure proper adhesion to the substrate.

SEM imaging was executed with a HITACHI SU8230 at 5 kV using secondary electron (SE) detection. Microscope imaging was conducted on a Keyence VHX-5000 Digital Microscope.

A Brookfield™ Rheometer was used to measure the rheology of the pastes.

Resistance of the printed connections was measured with a 6<sup>1</sup>/<sub>2</sub> digit Keysight 32251, a multimeter using a 4-wire sensing method in the range of 0–100 Ω. Error bars presented on the figures were calculated as standard deviations of the average resistance values of 8 measured samples. The surface morphology was measured with a BRUKER DektakXT profilometer: of the screen printed layer, the AJP layer, and the profile of hybrid connection (where the AJP lines cover the screen printed ones or where the paste layer covered the ink print). For each print, three individual samples were tested and displayed on the figures in three colors. Measurement resolution was 50 points of measurement per 1 μm of the sample. The measurement length was 600 μm (AJP, hybrid) and 1400 μm (screen).

For the mechanical fatigue tests, a dedicated machine was constructed (Figure 3). The device sets fatigue cycles at a frequency of 10 cycles/s. The samples were bent inwards (the side where the print was), with a bending radius of approximately 15 mm. The resistance of each sample was tested before and after a 30-min mechanical fatigue test which is equivalent to about 18,000 bending cycles per sample.

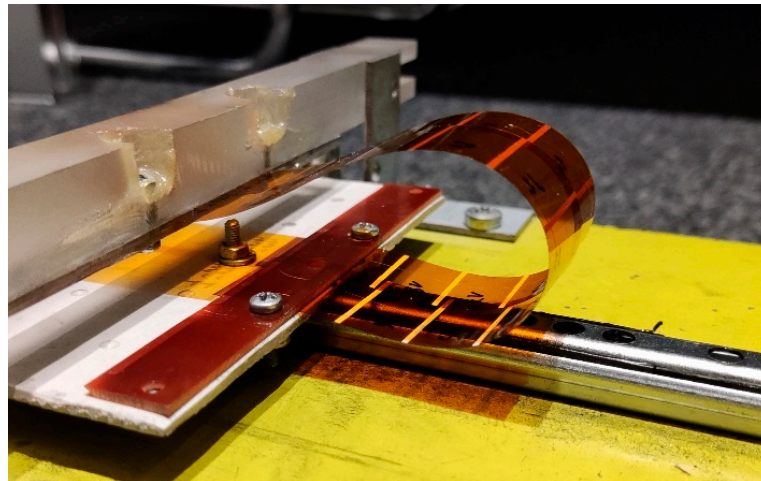


**Figure 3.** The machine made for mechanical fatigue testing: the sample bent on the machine.

### 3. Results and Discussion

#### 3.1. Hybrid Connections

The printed hybrid connections (Figure 4) were named and listed in Table 1. For the purpose of distinguishing between the different manufacturing processes, it was important to investigate if the qualities of prints with screen printed layers deposited on top of the AJP layers were comparable with the connections where AJP layers were printed on top of the screen printed ones. Most prints were conducted with two annealing processes after subsequent printing stages. Hybrid connections with a singular annealing process were also tested and compared with those with two annealing processes. The singular annealing

was conducted for the connections where AJP prints were deposited on top of the screen printed layers. Two- and four-layer AJP prints were prepared and tested.

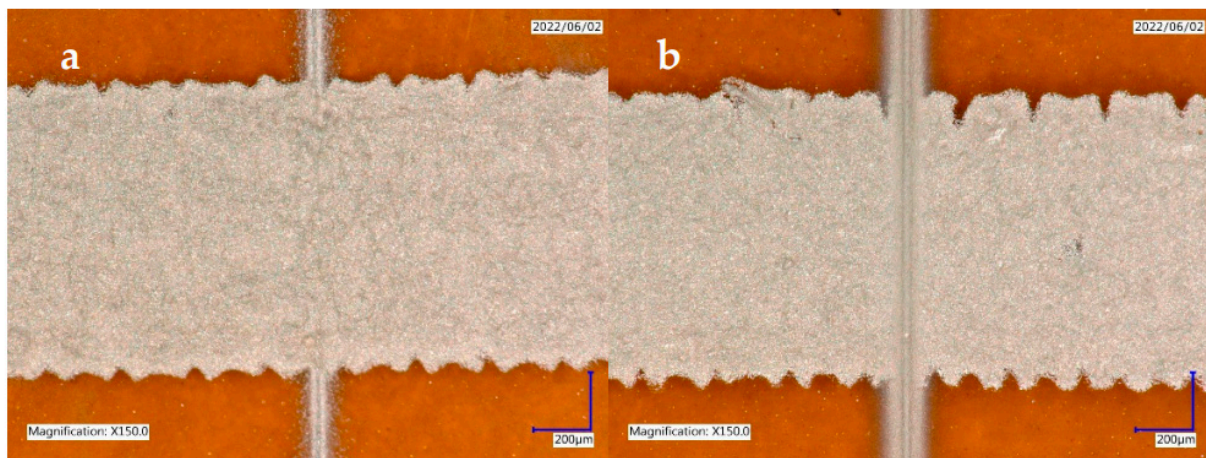


**Figure 4.** Images of printed hybrid connections. (a) a connection where PMMA-based paste was printed on top of a UTD40X 4-layer print; (b) a connection where UTD40X 4-layer print was printed on top of the PMMA-based print.

**Table 1.** An overview of hybrid connections that were prepared and tested.

Connection Name	Top Print	Bottom Print	Annealing between Prints	Amount of AJP Layers
UTD_PMMA_2	UTDots Ag40X	PMMA-based silver paste	yes	2 layers
UTD_PMMA_4	UTDots Ag40X	PMMA-based silver paste	yes	4 layers
UTD_PMMA_1a_2	UTDots Ag40X	PMMA-based silver paste	no	2 layers
UTD_PMMA_1a_4	UTDots Ag40X	PMMA-based silver paste	no	4 layers
PMMA_UTD_2	PMMA-based silver paste	UTDots Ag40X	yes	2 layers
PMMA_UTD_4	PMMA-based silver paste	UTDots Ag40X	yes	4 layers
UTD_1010_2	UTDots Ag40X	LOCTITE® ECI 1010 silver paste	yes	2 layers
UTD_1010_4	UTDots Ag40X	LOCTITE® ECI 1010 silver paste	yes	4 layers
UTD_1010_1a_2	UTDots Ag40X	LOCTITE® ECI 1010 silver paste	no	2 layers
UTD_1010_1a_4	UTDots Ag40X	LOCTITE® ECI 1010 silver paste	no	4 layers
1010_UTD_2	LOCTITE® ECI 1010 silver paste	UTDots Ag40X	yes	2 layers
1010_UTD_4	LOCTITE® ECI 1010 silver paste	UTDots Ag40X	yes	4 layers
UTD_PMMA_2	UTDots Ag40X	PMMA-based silver paste	yes	2 layers

Differences in the AJP lines can be observed (Figure 4). Despite identical printing parameters, this can sometimes occur with AJP due to the change in ink volume during the printing process and therefore different atomization. The print quality does not crucially affect the properties of the print other than visually.

### 3.2. SEM Imaging

#### 3.2.1. Screen Printed Layers

LOCTITE® ECI 1010 and PMMA-based paste share a similar silver flake size (2–8 µm). However, there is a difference in leveling between the materials. While 1010 tends to level easily after a one-layer print, PMMA is left with distinguishable differences in layer height

resulting from a higher accumulation of material in places related to the position of the openings in the screen (Figure 5). The difference in levelling is the result of higher viscosity of the PMMA-based paste while in the slump, the low shear rate area (Figure 2). This also results from greater thixotropy of the PMMA-based paste [32] when compared to ECI 1010.

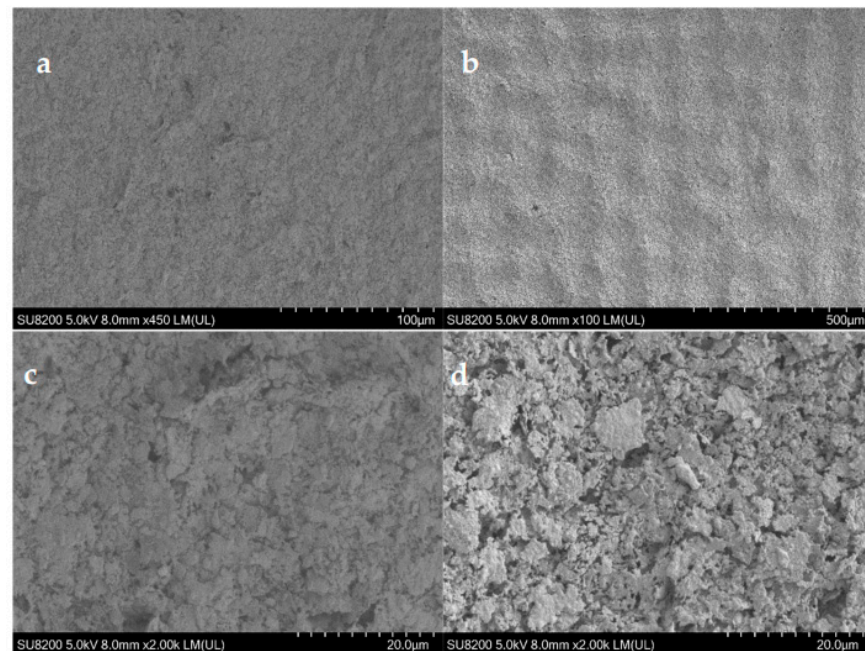


**Figure 5.** SEM image of the screen printed layers: (a) LOCTITE® ECI 1010; (b) PMMA-based silver paste; (c) ECI 1010 image of the flakes; (d) PMMA image of the flakes.

### 3.2.2. Aerosol Jet® Printed Layers

The lines were printed with AJP ink UTDots Ag40X. While annealing at 250 °C, the silver nanoparticle grains in the deposited ink layer tend to accumulate to form unified layers in a porous structure resulting from the sintering process (Figure 6). This means that silver particles have sintered well.

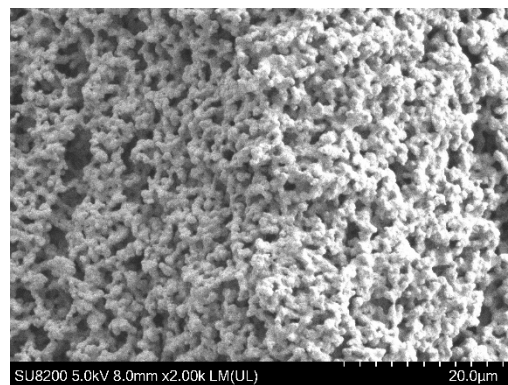


**Figure 6.** SEM image of the AJP layer printed with UTDots Ag40X with a visible high-roughness structure.

### 3.2.3. Hybrid Printing

The SEM imaging showed no significant difference between the material combinations. For the connections with AJP print used as the top layer, there can be seen a bridging between the sintered silver ink with the screen-printed silver flakes resulting in a well-established connection between the layers (Figure 7a,b).

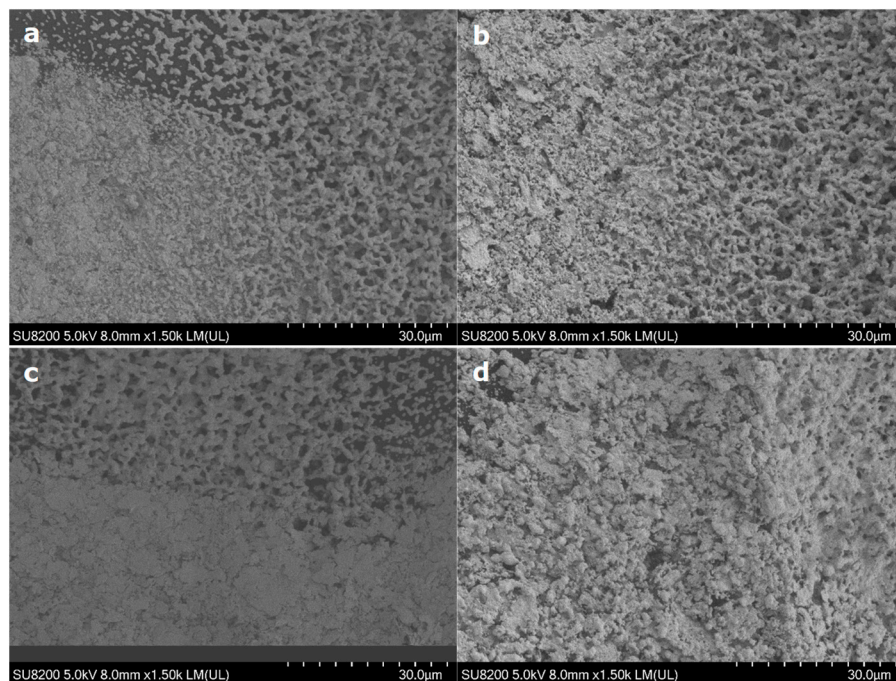


**Figure 7.** SEM images of hybrid connections: (a) UTD40X top layer on ECI 1010; (b) UTD40X top layer on PMMA; (c) ECI 1010 top layer on UTD40X; (d) PMMA top layer on UTD40X.

The combinations with pastes printed as the top layer on the AJP lines proved that screen printing layers on top of AJP prints does not impose any significant, observable damage to the AJP lines (Figure 7c,d).

### 3.3. Surface Morphology—Profilometer Results

#### 3.3.1. Screen Printed Layers

The profiles of the screen-printed layers were measured and analyzed. The average height of the profile was measured, and the average max height was calculated and presented in Table 2.

**Table 2.** Results of profilometer measurements for screen printed layers. Average values were calculated from 3 measurements.

Paste	Avg. Height (µm)	Std. Dev. of Avg. Height (µm)	Avg. Max. Height (µm)	Std. Dev. of Avg. Max. Height (µm)
ECI 1010	3.28	0.82	5.73	1.39
PMMA	12.34	2.82	18.83	3.60

In Figure 8, the profiles of the screen-printed layers, specifically the PMMA-based paste and LOCTITE® ECI 1010, exhibit noticeable differences in height and roughness. The PMMA-based paste demonstrates a nearly four-fold higher profile compared to LOCTITE® ECI 1010. Upon closer observation, it can be observed that the profile of the PMMA-based paste exhibits ripples, as discussed in Section 3.1. This effect is attributed to the higher viscosity of the paste during the slump, which leads to poor leveling. Although this could potentially impact the effectiveness of the hybrid connection, further research indicated that this issue did not occur. Despite the disparities in profile heights and roughness between the two pastes, subsequent investigations confirmed that it did not compromise the performance of the hybrid connection.

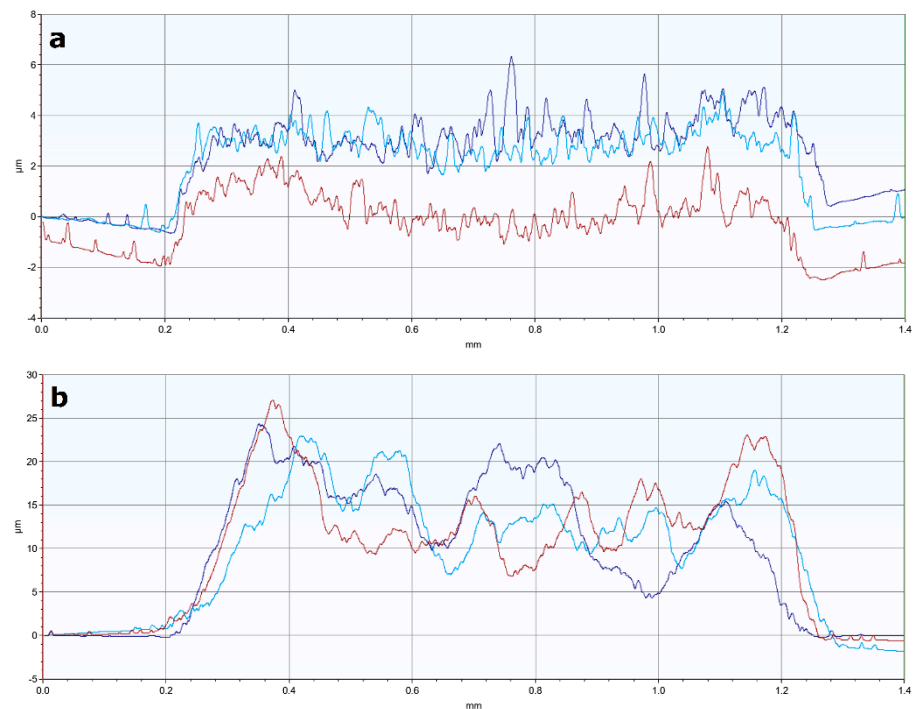


**Figure 8.** Profiles of the screen-printed layers' surface: (a) LOCTITE® ECI 1010 with good leveling resulting from lower viscosity; (b) PMMA-based silver paste with a noticeable leveling issue resulting from higher viscosity paste. Three samples of each paste were measured and displayed together (as differently colored plots on each subplot).

### 3.3.2. Aerosol Jet® Printed Lines

AJP lines were deposited on the Kapton substrate. One-, two-, and four-layer prints were compared (Figure 9). A linear trend relation between the number of layers and the average maximum height of the print measured was observed (Figure 10). This means that the printing process was conducted with the correct printing parameters.

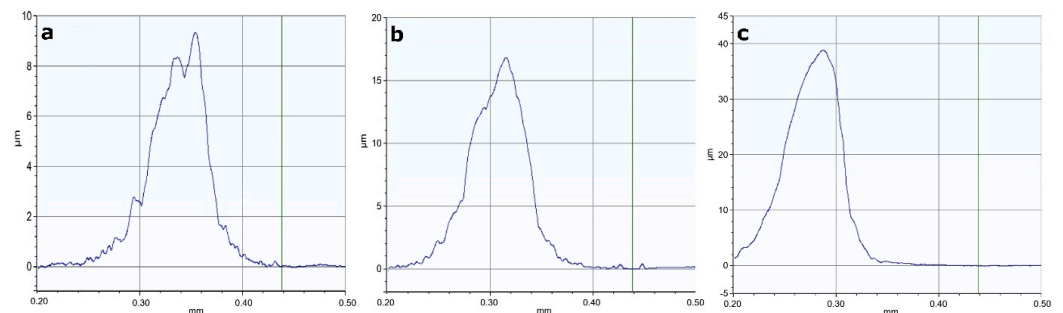


**Figure 9.** Profiles of AJP printed lines: (a) 1-layer print, height: 9  $\mu\text{m}$ ; (b) 2-layer print, height: 17  $\mu\text{m}$ ; (c) 3-layer print, height: 37  $\mu\text{m}$ .

### 3.3.3. Hybrid Printing

The profiles of screen-printed layers on top of the AJP printed lines showed slightly visible changes in morphology with the PMMA-based paste, meaning there is presumably a thinner layer of paste atop the AJP print (Figure 11a). The combination with ECI 1010 paste has a distinguishable peak where the paste covers the AJP lines (Figure 11b). This means that the paste covers the AJP print and builds up atop it, therefore sustaining the thickness of the screen-printed layer. This difference between the materials results from the rheological properties of the pastes used (Figure 2).

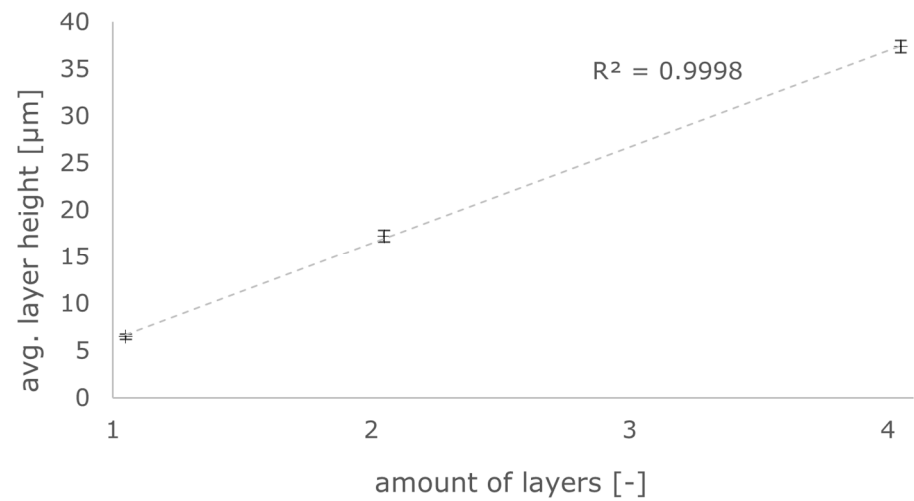


**Figure 10.** The plot of the average layer height of UTD40X prints over the number of printed layers. The error bars presented are the value of the standard deviation of average calculated based on 3 measurements conducted for each sample.

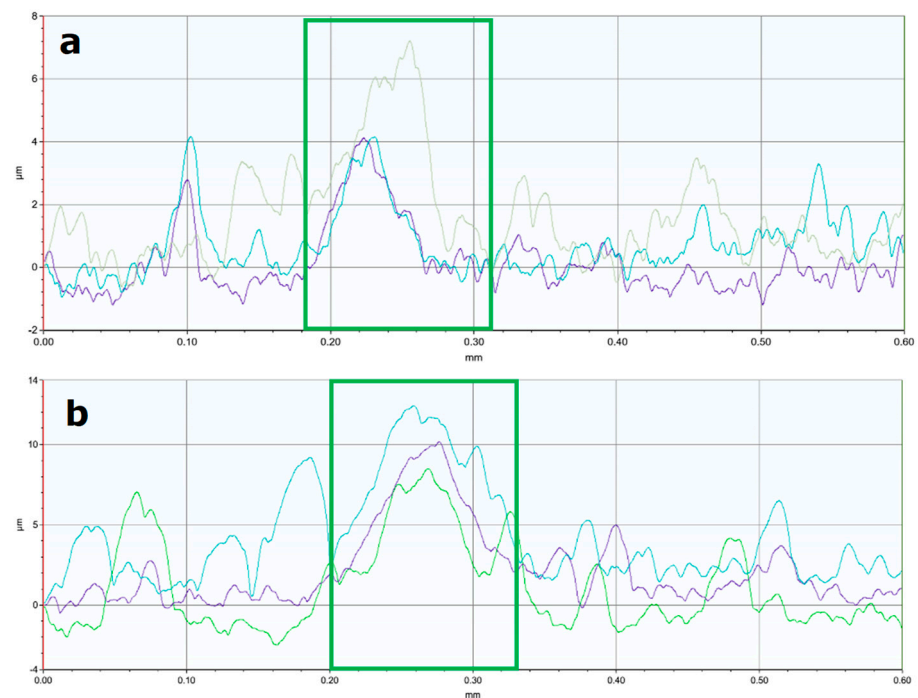


**Figure 11.** Profiles of hybrid-printed connections with 4-layer AJP printed lines. (a) Three measurements of PMMA-based paste on top of UTD40X lines; (b) Three measurements of LOCTITE® ECI 1010 on top of UTD40X lines. Three samples of each paste were measured and displayed together (as differently colored plots on each subplot). The green box points the area where the AJP layer is located.

In hybrid connections, where the bottom layer was screen printed, the peak from AJP printed lines is significant. Due to leveling problems with the PMMA-based silver paste described earlier, one-layer prints can hardly be distinguished on the profile. However, the four-layer AJP prints proved to be well-recognizable on the surface of the screen prints (Figure 12).

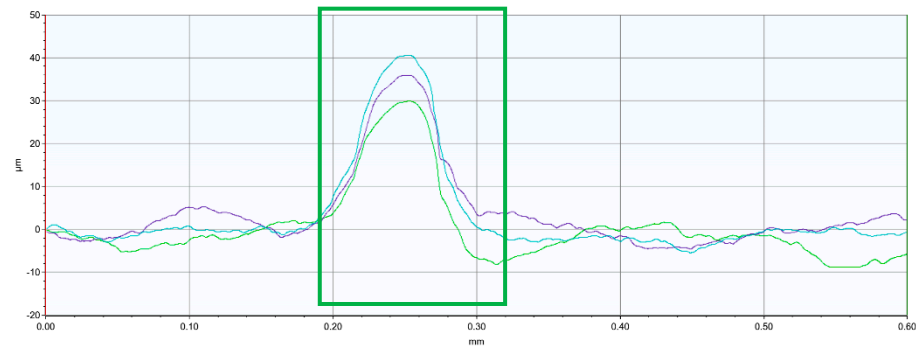


**Figure 12.** Profiles of the hybrid connection with a 4-layer UTD40X print on top of the PMMA-based silver paste (3 measurements). The AJP peak of around 30–40  $\mu\text{m}$  is well recognizable against the screen-printed layer. Three samples of each paste were measured and displayed together (as differently colored plots on each subplot). The green box points the area where the AJP layer is located.

### 3.4. Measurements of Electric Properties of the Hybrid Connections

Electric measurements were conducted on hybrid connections as described in Section 3.1. The connections with a singular annealing process (PMMA\_UTD\_1a, 1010\_UTD\_1a) were reviewed in Section 3.6. The average values were calculated based on eight samples for specific hybrid connections.

The combination of UTD40X AJP ink with the PMMA-based screen printing silver paste (Figure 13) presented the lowest resistance of all researched connections for the connections with four-layer AJP ink on top of the PMMA paste (UTD\_PMMA\_4). The resistance values of  $1.47 \pm 0.06 \Omega$  for the connection UTD\_PMMA\_4 and  $1.79 \pm 0.02 \Omega$  for the connection UTD\_PMMA\_1a\_4 provide the reason to believe the connections were properly established. The connection PMMA\_UTD\_4, with PMMA-based paste printed on top of the four-layer AJP lines, has a significantly higher average resistance of  $12.32 \pm 3.42 \Omega$  than the other connections. This may result from the fact that AJP ink being deposited on top of the paste has a greater opportunity to establish contact with the silver paste while annealing the ink layer. The same is not true for the connections with paste applied as the top layer, as it is deposited on an already sintered AJP printed line with no polymeric carrier, therefore having difficulties in establishing a new connection. The spread of the results is also significantly larger. This is presumably due to less stability and control during the annealing process.

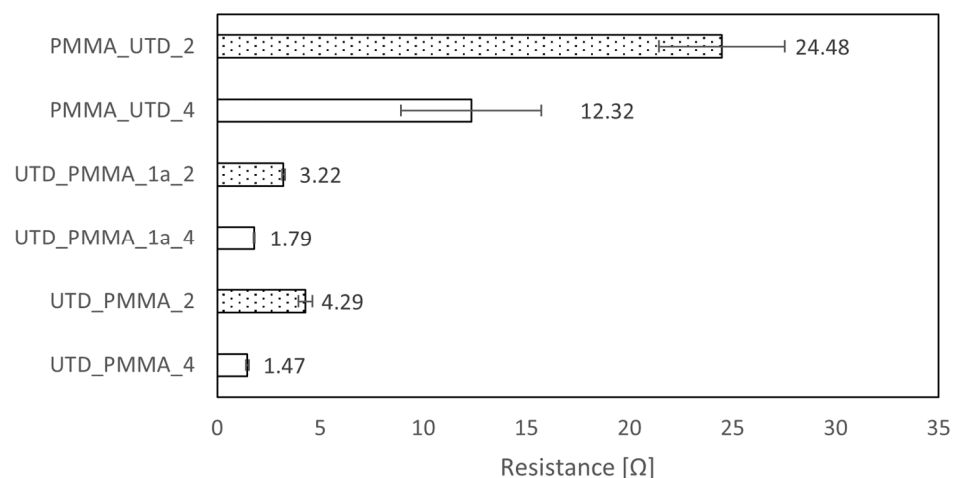


**Figure 13.** Hybrid connections AJP silver ink UTDots Ag40X and the PMMA-based silver paste for screen printing. The bars corresponding to the connections with the two-layer aerosol print have been dotted. A description of the electric measurements method can be found in Section 2.1.

The combination of UTD40X AJP ink with LOCTITE® ECI 1010 screen printing silver paste presented different results from the connections with the PMMA-based paste (Figure 14). There are similar results of resistance of around 5  $\Omega$  for all connections with a four-layer AJP print. While the connection with screen printed paste applied as the top layer (1010\_UTD\_4) has the highest resistance of  $5.68 \pm 0.19 \Omega$ , it is a similar value to the lowest resistance of  $4.95 \pm 0.04 \Omega$  of the connection UTD\_1010\_1a\_4 with a singular annealing process. Considering the connections with a two-layer AJP print, 1010\_UTD\_2 presents a higher resistance than the other connections. This may be due to instabilities in the AJP printing process which tend to be eliminated with multiple-layer printing.

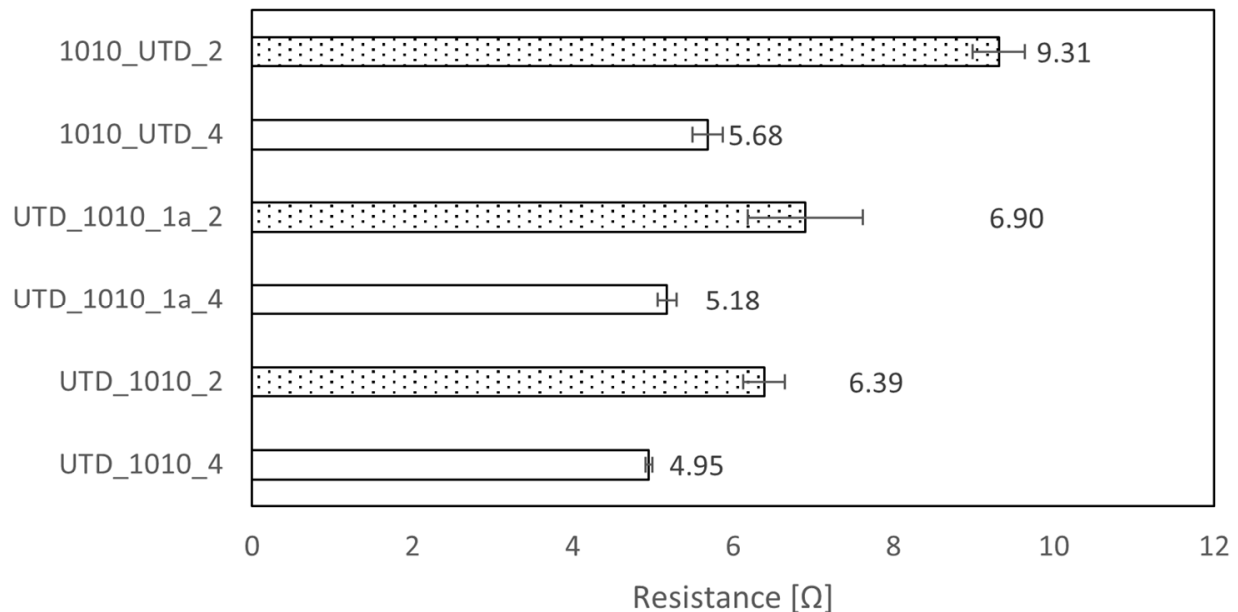


**Figure 14.** Hybrid connections AJP silver ink UTDots Ag40X and LOCTITE® ECI 1010 paste for screen printing. The bars corresponding to the connections with the two-layer aerosol print have been dotted. A description of the electric measurements method can be found in Section 2.1.

### 3.5. Mechanical Fatigue Test

To investigate the mechanical durability of the hybrid connection as a solution for application in flexible electronics the mechanical fatigue test of 18,000 bending cycles was conducted. To analyze the durability of the hybrid connections, resistance of the samples was measured before the mechanical fatigue test and after 18,000 bending cycles, and the values were compared.

No significant changes in resistance were observed for the connections of PMMA paste with UTD aerosol lines (Figure 15). A maximum increase in resistance (around 3%) was observed for the hybrid connection PMMA\_UTD\_2. It is worth mentioning that some of the connections maintained the values from before the mechanical fatigue tests after bending cycles. This is proof that hybrid connections of tested materials are durable and can be used in vast applications of flexible electronics.

Similar results were obtained for hybrid connections of 1010 paste with UTD aerosol lines (Figure 16). In this instance, the hybrid connections exhibited minor decreases and increases in resistance after the bending cycles. The changes in average resistance values were no more than 1%, which may be compared to statistical or apparatus error. Connections of the two materials exhibit major durability to the bending cycles and therefore can be used in applications of flexible electronics.

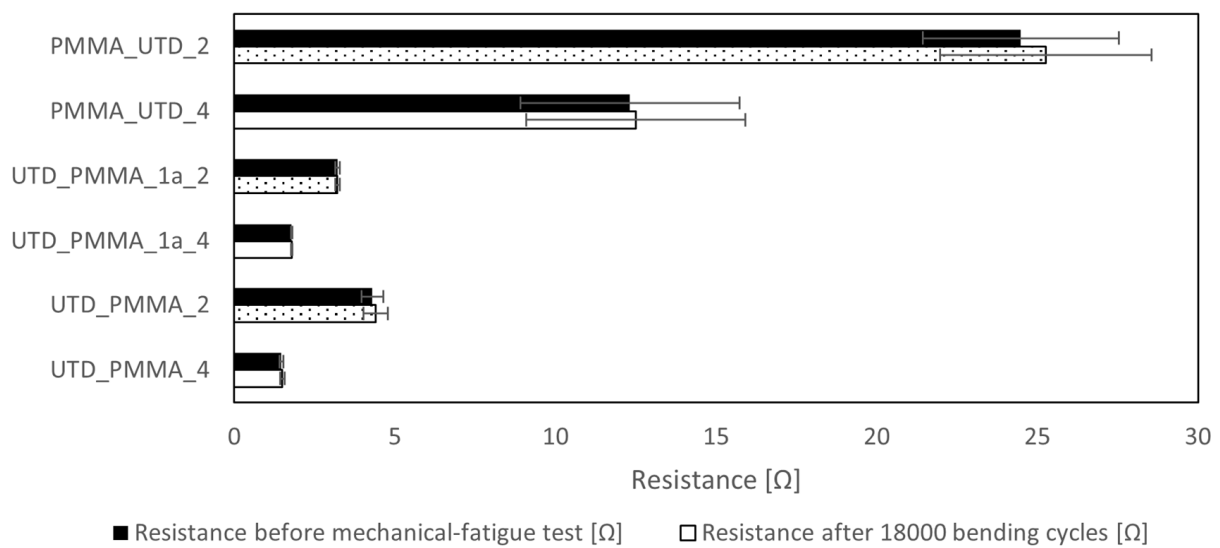


**Figure 15.** Results of the average resistance values before and after the mechanical fatigue tests for hybrid connections with PMMA-based paste and UTDots Ag40X AJP ink. The bars corresponding to the connections with the two-layer aerosol print have been dotted. A description of the electric measurements method can be found in Section 2.1.

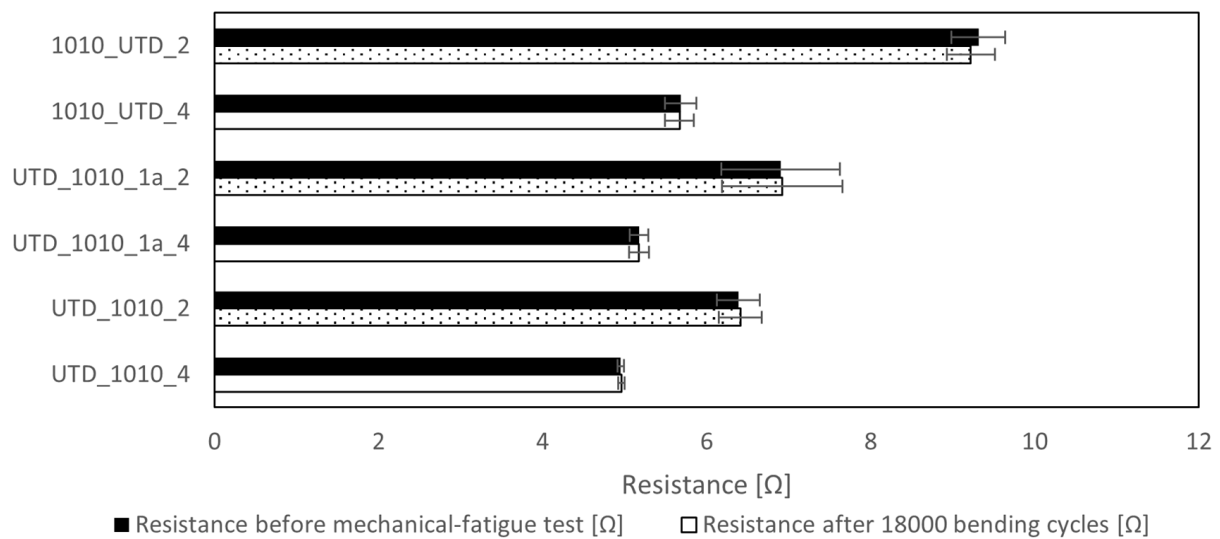


**Figure 16.** Results of the average resistance values before and after the mechanical fatigue tests for hybrid connections with LOCTITE® ECI 1010 paste and UTDots Ag40X AJP ink. The bars corresponding to the connections with the two-layer aerosol print have been dotted. A description of the electric measurements method can be found in Section 2.1.

### 3.6. Discussion of Hybrid Printing with a Singular Annealing Process

Annealing processes tend to require a significant amount of time on the production line. Therefore, comparisons were made between a hybrid connection with an annealing process after screen printing and AJP, as well as a connection where there is only one annealing process after both prints are deposited. No significant differences were observed with SEM imaging (Figure 17).

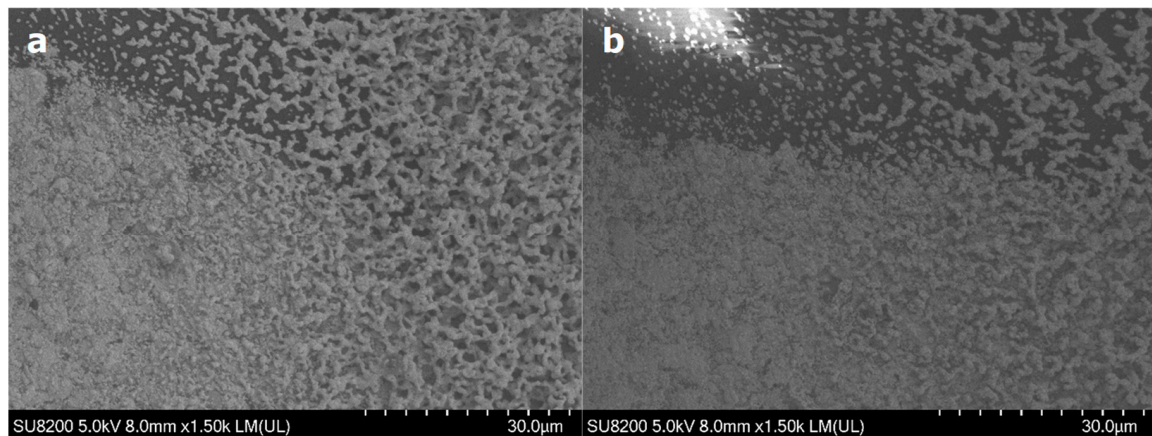


**Figure 17.** SEM images of a hybrid connection with UTD40X printed atop ECI 1010 paste: (a) hybrid connection with double annealing after each print; (b) hybrid connection with a singular annealing process after both prints.

The profilometer measurements also resulted in similar profiles for both annealing methods (Figure 18).

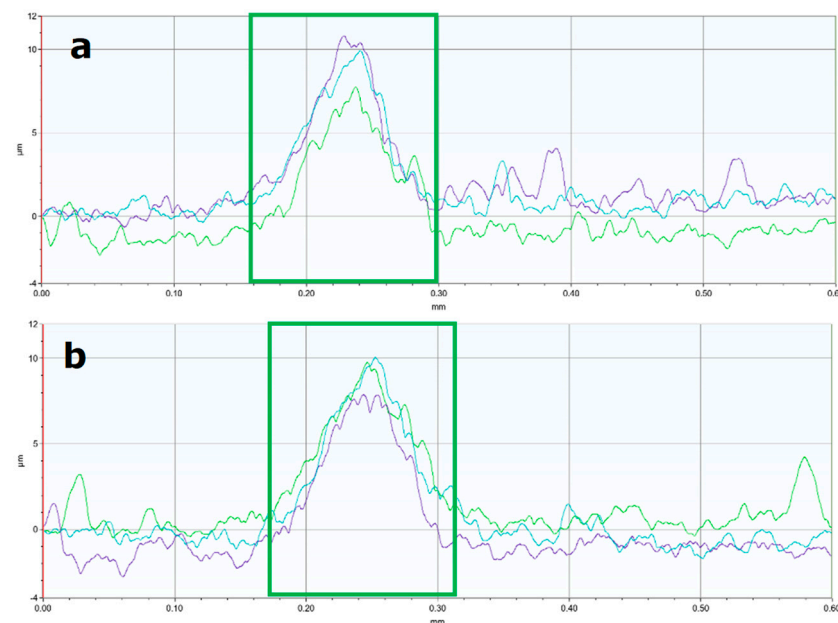


**Figure 18.** Profiles of hybrid-printed connections with 4-layer AJP printed lines on top of ECI 1010 silver paste. (a) hybrid connection with double annealing after each print; (b) hybrid connection with a singular annealing process after both prints. Three samples of each paste were measured and displayed together (as differently colored plots on each subplot). The green box points the area where the AJP layer is located.

Similar values of resistance were obtained for both connections with a singular annealing process as well as the connections with a double annealing process (Figures 13 and 14). Both in the connection of PMMA paste with UTD ink, and in the connection with 1010 paste, the samples with double annealing achieved lower resistance. This may be due to better sintering of silver flakes and particles in double annealing time.

The mechanical fatigue tests raised no concerns as to the mechanical durability of the hybrid connections with a singular annealing process, even when compared to the hybrid connections with double annealing processes.

#### 4. Conclusions

In this study, hybrid printing was introduced as a combination of aerosol jet printing and screen printing methods. Materials for the research were selected due to them being used in ongoing research for the applications in flexible sensors. UTDots Ag40X ink was used in the aerosol jet printing process and two pastes were selected for screen printing: widely used, commercially available paste LOCTITE<sup>®</sup> ECI 1010 and PMMA-based silver paste manufactured for the research. Three printing combinations were checked: aerosol lines printed on top of the screen printed layers with an annealing process after each print; aerosol lines printed on top of the screen printed ones with a singular annealing process after both prints; screen printed lines printed on top of the aerosol ones with annealing after both prints.

An investigation of the properties recognized as most significant in the research was conducted. The SEM imaging and profilometer measurements proved the integrity of the hybrid connections. The observations of hybrid printed connections led to a conclusion that screen printing layers on top of AJP lines is possible without damaging the AJP print. However, electric measurements of the samples demonstrated a higher resistance of the connections ( $12.32 \pm 3.42 \Omega$  for PMMA\_UTD\_4) when compared to the ones with aerosol lines printed as the top layer ( $1.47 \pm 0.06 \Omega$  for UTD\_PMMA\_4).

The electric measurements were conducted to compare the samples with double annealing processes to the ones with a singular annealing process after both prints. The first achieved slightly lower resistance values ( $1.47 \pm 0.06 \Omega$  for UTD\_PMMA\_4) than the ones with singular annealing after both prints ( $1.79 \pm 0.02 \Omega$  for UTD\_PMMA\_1a\_4). Regarding the mechanical tests and morphology, single-annealing-process connections showed similar performance to their counterparts with double annealing.

All the researched hybrid connections proved to be exceptionally durable (showing less than 5% change in resistance) and conductive, some having resistance values of even  $1.5 \Omega$ . The achieved mechanical strength is especially important in flexible sensor solutions.

The concept of hybrid printing as a combination of aerosol jet printing and screen printing was introduced as a novel solution for flexible printed electronics applications, such as flexible sensors. This work proved that hybrid connections preserve functionality of both electronics printing techniques without any significant reduction in durability and conductivity. The results provide recognition of the potential in the presented solution and provide a basis for the future research with diverse types of functional phase materials in the hybrid combinations.

**Author Contributions:** Conceptualization, J.K. and D.B.; methodology, D.B.; software, D.B.; validation, J.K., J.D. and M.J.; formal analysis, D.B. and J.K.; investigation, D.B., T.R. and I.W.; resources, J.K. and D.J.; data curation, J.K.; writing—original draft preparation, D.B. and J.K.; writing—review and editing, J.K. and J.D.; visualization, D.B.; supervision, J.K.; project administration, J.K.; funding acquisition, M.J. All authors have read and agreed to the published version of the manuscript.

**Funding:** This research was funded by European Union's Horizon 2020 Research and Innovation Programme under the Grant Agreement no: 101008701 (EMERGE, H2020-INFRAIA-2020-1).

**Conflicts of Interest:** The authors declare no conflict of interest.

#### References

1. Johnson, L.S.J.; Bechtold, D.A.; Casson, A.J. Screen Printed, Skin-compliant Sensors for Mouse Electrocardiography. In Proceedings of the 2022 IEEE International Conference on Flexible and Printable Sensors and Systems (FLEPS), Vienna, Austria, 10–13 July 2022; pp. 1–4. [CrossRef]
2. Ives, L.; Pace, A.; Bor, F.; Jing, Q.; Wade, T.; Cama, J.; Khanduja, V.; Kar-Narayan, S. Conformable and robust force sensors to enable precision joint replacement surgery. *bioRxiv* **2021**. [CrossRef]
3. Krzemiński, J.; Dominiczak, J.; Baraniecki, D.; Janczak, D.; Raczyński, T.; Ostapko, J.; Jakubowska, M. Printability of Collecting Electrode Using AJP for New Construction of Photovoltaic Device. *Crystals* **2021**, *11*, 1184. [CrossRef]
4. Erath, D.; Filipović, A.; Retzlaff, M.; Goetz, A.K.; Clement, F.; Biro, D.; Preu, R. Advanced screen printing technique for high definition front side metallization of crystalline silicon solar cells. *Sol. Energy Mater. Sol. Cells* **2010**, *94*, 57–61. [CrossRef]

5. Janczak, D.; Zych, M.; Raczyński, T.; Dybowska-Sarapuk, Ł.; Peplowski, A.; Krzemiński, J.; Sosna-Głębska, A.; Znajdek, K.; Sibiński, M.; Jakubowska, M. Stretchable and Washable Electroluminescent Display Screen-Printed on Textile. *Nanomaterials* **2019**, *9*, 1276. [CrossRef]
6. Inzelberg, L.; Pur, M.D.; Schliske, S.; Rödlmeier, T.; Granoviter, O.; Rand, D.; Steinberg, S.; Hernandez-Sosa, G.; Hanein, Y. Printed facial skin electrodes as sensors of emotional affect. *Flex. Print. Electron.* **2018**, *3*, 045001. [CrossRef]
7. Jing, Q.; Choi, Y.S.; Smith, M.; Ou, C.; Busolo, T.; Kar-Narayan, S. Freestanding Functional Structures by Aerosol-Jet Printing for Stretchable Electronics and Sensing Applications. *Adv. Mater. Technol.* **2019**, *4*, 1900048. [CrossRef]
8. Eskandarinezhad, S.; Yusuf, M. An overview of materials, processing, and applications for wearable electronics. *J. Compos. Compd.* **2021**, *3*, 275–290. [CrossRef]
9. Ahmad, J.; Andersson, H.; Siden, J. Screen-Printed Piezoresistive Sensors for Monitoring Pressure Distribution in Wheelchair. *IEEE Sens. J.* **2019**, *19*, 2055–2063. [CrossRef]
10. Zhou, R.; Li, J.; Jiang, H.; Li, H.; Wang, Y.; Briand, D.; Camara, M.; Zhou, G.; de Rooij, N.F. Highly transparent humidity sensor with thin cellulose acetate butyrate and hydrophobic AF1600X vapor permeating layers fabricated by screen printing. *Sens. Actuators B Chem.* **2019**, *281*, 212–220. [CrossRef]
11. Dubourg, G.; Segkos, A.; Katona, J.; Radović, M.; Savic, S.; Niarchos, G.; Tsamis, C.; Crnojević-Bengin, V. Fabrication and Characterization of Flexible and Miniaturized Humidity Sensors Using Screen-Printed TiO<sub>2</sub> Nanoparticles as Sensitive Layer. *Sensors* **2017**, *17*, 1854. [CrossRef]
12. Albrecht, A.; Salmeron, J.F.; Becherer, M.; Lugli, P.; Rivadeneyra, A. Screen-Printed Chipless Wireless Temperature Sensor. *IEEE Sens. J.* **2019**, *19*, 12011–12015. [CrossRef]
13. Ferri, J.; Llopis, R.L.; Moreno, J.; Civera, J.I.; Garcia-Breijo, E. A Wearable Textile 3D Gesture Recognition Sensor Based on Screen-Printing Technology. *Sensors* **2019**, *19*, 5068. [CrossRef]
14. Wu, K.; Hong, J.; Qi, X.; Ye, H.; Li, Z.; Cong, C.; Liu, J.; Li, X.; Ryu, K.Y.; Nam, S.Y.; et al. Screen printing of silver nanoparticles on the source/drain electrodes of organic thin-film transistors. *Org. Electron.* **2022**, *106*, 106524. [CrossRef]
15. Stoukatch, S.; Laurent, P.; Dricot, S.; Axisa, F.; Seronveaux, L.; Vandormael, D.; Beeckman, E.; Heusdens, B.; Destine, J. Evaluation of Aerosol Jet Printing (AJP) technology for electronic packaging and interconnect technique. In Proceedings of the 2012 4th Electronic System-Integration Technology Conference, Amsterdam, The Netherlands, 17–20 September 2012; pp. 1–5. [CrossRef]
16. Hyun, W.J.; Secor, E.B.; Hersam, M.C.; Frisbie, C.D.; Francis, L.F. High-Resolution Patterning of Graphene by Screen Printing with a Silicon Stencil for Highly Flexible Printed Electronics. *Adv. Mater.* **2015**, *27*, 109–115. [CrossRef]
17. Lu, S.; Cardenas, J.A.; Worsley, R.; Williams, N.X.; Andrews, J.B.; Casiraghi, C.; Franklin, A.D. Flexible, Print-in-Place 1D–2D Thin-Film Transistors Using Aerosol Jet Printing. *ACS Nano* **2019**, *13*, 11263–11272. [CrossRef]
18. Jing, Q.; Pace, A.; Ives, L.; Husmann, A.; Ćatić, N.; Khanduja, V.; Cama, J.; Kar-Narayan, S. Aerosol-jet-printed, conformable microfluidic force sensors. *Cell Rep. Phys. Sci.* **2021**, *2*, 100386. [CrossRef]
19. Wilkinson, N.J.; Smith, M.A.A.; Kay, R.W.; Harris, R.A. A review of aerosol jet printing—A non-traditional hybrid process for micro-manufacturing. *Int. J. Adv. Manuf. Technol.* **2019**, *105*, 4599–4619. [CrossRef]
20. Aerosol Jet<sup>®</sup> Printed Electronics Overview. Available online: [https://www.optomec.com/wp-content/uploads/2014/04/AJ\\_Printed\\_Electronics\\_Overview\\_whitepaper.pdf](https://www.optomec.com/wp-content/uploads/2014/04/AJ_Printed_Electronics_Overview_whitepaper.pdf) (accessed on 20 January 2023).
21. Vella, S.; Smithson, C.; Halfyard, K.; Shen, E.; Chrétien, M. Integrated capacitive sensor devices aerosol jet printed on 3D objects. *Flex. Print. Electron.* **2019**, *4*, 045005. [CrossRef]
22. Hedges, M.; Marin, A.B. 3D Aerosol Jet<sup>®</sup> Printing-Adding Electronics Functionality to RP/RM. In Proceedings of the DDMC 2012 Conference, Berlin, Germany, 14–15 March 2012.
23. Krzemiński, J.; Jakubowska, M.; Kanthamneni, A.; Wagner, D.; Detert, M.; Schmidt, B. Pads and microscale vias with aerosol jet printing technique. In Proceedings of the 2017 21st European Microelectronics and Packaging Conference (EMPC) & Exhibition, Warsaw, Poland, 10–13 September 2017; pp. 1–4. [CrossRef]
24. Bücher, T.; Huber, R.; Eschenbaum, C.; Mertens, A.; Lemmer, U.; Amrouch, H. Printed temperature sensor array for high-resolution thermal mapping. *Sci. Rep.* **2022**, *12*, 14231. [CrossRef]
25. Janczak, D.; Peplowski, A.; Wroblewski, G.; Gorski, L.; Zwierkowska, E.; Jakubowska, M. Investigations of Printed Flexible pH Sensing Materials Based on Graphene Platelets and Submicron RuO<sub>2</sub> Powders. *J. Sens.* **2017**, *2017*, 2190429. [CrossRef]
26. Cao, C.; Andrews, J.B.; Franklin, A.D. Completely Printed, Flexible, Stable, and Hysteresis-Free Carbon Nanotube Thin-Film Transistors via Aerosol Jet Printing. *Adv. Electron. Mater.* **2017**, *3*, 1700057. [CrossRef]
27. Yu, X.; Gong, X.; Podder, C.; Ludwig, B.; Chen, I.-M.; Shou, W.; Alvidrez, A.; Chen, G.; Huang, X.; Pan, H. Additive Manufacturing of Sandwich-Structured Conductors for Applications in Flexible and Stretchable Electronics. *Adv. Eng. Mater.* **2021**, *23*, 2100286. [CrossRef]
28. Mahajan, A.; Frisbie, C.D.; Francis, L.F. Optimization of Aerosol Jet Printing for High-Resolution, High-Aspect Ratio Silver Lines. *ACS Appl. Mater. Interfaces* **2013**, *5*, 4856–4864. [CrossRef]
29. Smocot, S.; Zhang, Z.; Zhang, L.; Guo, S.; Cao, C. Printed flexible mechanical sensors. *Nanoscale* **2022**, *14*, 17134–17156. [CrossRef] [PubMed]
30. Phero, T.L.; Novich, K.A.; Johnson, B.C.; McMurtrey, M.D.; Estrada, D.; Jaques, B.J. Additively manufactured strain sensors for in-pile applications. *Sens. Actuators A Phys.* **2022**, *344*, 113691. [CrossRef]

31. Skarżyński, K.; Krzemiński, J.; Jakubowska, M.; Słoma, M. Highly conductive electronics circuits from aerosol jet printed silver inks. *Sci. Rep.* **2021**, *11*, 18141. [[CrossRef](#)]
32. Hong, H.; Jiyong, H.; Moon, K.-S.; Yan, X.; Wong, C.-P. Rheological properties and screen printability of UV curable conductive ink for flexible and washable E-textiles. *J. Mater. Sci. Technol.* **2021**, *67*, 145–155. [[CrossRef](#)]

**Disclaimer/Publisher’s Note:** The statements, opinions and data contained in all publications are solely those of the individual author(s) and contributor(s) and not of MDPI and/or the editor(s). MDPI and/or the editor(s) disclaim responsibility for any injury to people or property resulting from any ideas, methods, instructions or products referred to in the content.